

- S. J. Benkovic, K. D. Janda, R. A. Lerner, *Science* **252**, 680 (1991)] cannot be compared with those of our catalysts because these antibodies catalyze second-order reactions. Our uncatalyzed reaction is pseudo-first order because we assay the ligation of stable substrate-template complexes.
17. M. Golomb and M. Chamberlin, *J. Biol. Chem.* **249**, 2858 (1974).
 18. The T7 RNA polymerase elongation rate was determined in 20 mM MgCl₂ at 37°C (17). Uncatalyzed oligonucleotide ligation proceeds at 7 × 10⁻⁷ per hour in 20 mM MgCl₂ at 25°C (Fig. 7) and generally four times faster at 37°C than at 25°C.
 19. D. Herschlag and T. R. Cech, *Biochemistry* **29**, 10159 (1990).
 20. M. Morl, I. Niemer, C. Schmelzer, *Cell* **70**, 803 (1992).
 21. G. F. Joyce and L. E. Orgel, in *The RNA World*, R. Gestland and J. Atkins, Eds. (Cold Spring Harbor Press, Cold Spring Harbor, NY, 1993), chap. 1.
 22. L. E. Orgel, *J. Theor. Biol.* **123**, 127 (1986).
 23. R. Lohrmann, *J. Mol. Evol.* **6**, 237 (1975).
 24. P. K. Bridson and L. E. Orgel, *J. Mol. Biol.* **144**, 567 (1980).
 25. T. Inoue and L. E. Orgel, *ibid.* **162**, 201 (1982).
 26. J. Ninio and L. E. Orgel, *J. Mol. Evol.* **12**, 91 (1978).
 27. D. P. Bartel and J. W. Szostak, in preparation.
 28. The 110-nt N72 DNA, 5'-AACACTATCCGACTG-GCACC-N72-CCTTGGTCAATTAGGATCC (Ban I and Sty I sites are italicized), was synthesized and gel-purified (yield, 150 μg). A 3:3:2:2 molar ratio of A, C, G, and T phosphoramidites was used to synthesize the 72 random positions to compensate for the faster coupling rates of G and T phosphoramidites. Primer extension experiments indicated that up to 79 percent of the gel-purified product had chemical lesions that block second-strand synthesis. Therefore, this synthesis yielded 31.5 μg of DNA that could be amplified by PCR (5.2 × 10¹⁴ different sequences). The 110-nt N76 DNA, 5'-CGGGACTCTGACCTTGG-N76-GGCA-CCTGTCCACGCTC, was synthesized, purified, and analyzed in the same manner and contained 96 μg of amplifiable DNA (1.6 × 10¹⁵ different sequences). The N72 and N76 pools were amplified in large (200 ml) PCR reactions for six and four cycles, respectively. After phenol extraction and precipitation, N72 DNA was cut with either Sty I (500 μg of DNA, 20,000 units of enzyme, 40-ml reaction) or Ban I (500 μg, 6000 units of enzyme, 20-ml reaction). N76 DNA was digested with both Sty I and Ban I. The N72-Sty I, N72-Ban I, and N76-Ban I-Sty I fragments were purified on a nondenaturing acrylamide gel. Ligation of the three fragments (3.5 nmol of each fragment, T4 DNA ligase, 1.1-ml reaction) was efficient and yielded predominantly the desired full-length three-piece product (80 percent yield). Pool 0 DNA was cloned and partial sequences of 11 randomly chosen clones indicated that the nucleotide distribution within the random-sequence segments fell within acceptable limits (A:C:G:T = 380:418:429:330 = 25:26:27:21).
 29. The sequence of pool 0 DNA is 5'-TTCTAATAC-GACTCACTATAGGAACACTATCCGACTGGCAC-N₇₂-CCTTGG-N₇₆-GGCACC-N₇₂-CCTTGGT-CATTAGGATCCCG (T7 promoter is italicized). The pool 0 RNA begins with the G immediately flanking the T7 promoter. Pool 0 DNA was amplified with 42- and 20-nt primers corresponding to the 5' and 3' constant regions, respectively.
 30. Pool RNA and a twofold molar excess of biotinylated DNA (5'-biotin-CGGGATCCTAATGAC-CAAGG) were denatured in water (80°C, 3 minutes) and allowed to cool briefly at room temperature before the addition of streptavidin-agarose (SA) binding buffer (30 mM Tris, pH 7.4, 500 mM NaCl, 1 mM EDTA, 0.25 percent NP-40, 0.1 percent SDS). After 5 minutes at room temperature, a suspension of SA beads (Sigma) in binding buffer was added; the mixture was rocked for 20 minutes, and then poured into a column for washing and buffer equilibration. In round 1, a total of 160 ml of SA suspension containing 18 ml of SA was added to a 40-ml annealing reaction mixture that contained 4 mg of pool 0 RNA. In later rounds, much less RNA and smaller volumes were used; by round 4, a 2-ml SA suspension was added to 0.25 ml of annealed pool.
 31. Synthetic DNA-RNA chimeric substrate oligonucleotides that contain a DNA tag sequence [(dA)₂₂, (dT)₂₂, or 5'-dAAGCATCTAAGCATCT-CAAGCAA] followed by the RNA sequence 5'-CCAGUC were used with their cognate oligonucleotide affinity columns [oligo(dT)-cellulose type 7 (Pharmacia), oligo(dA)-cellulose type 7 (Pharmacia), (dT)₂₅ magnetic beads, or dGAGATGCT-TAGATGCA-Teflon (Glen Research)], as indicated in Table 1 (italics indicate segments of complementarity).
 32. The selective PCR primers had the following DNA sequences (A)₂₂-CCAGTC, (T)₂₂-CCAGTC, and AAGCATCTAAGCATCTCAAGCA. Other primers were the same as those used in the pool 0 amplification (29).
 33. Although the pool RNA of rounds 6 to 10 was not immobilized on the agarose before the ligation reaction, the RNA was subjected to an annealing treatment that approximated the temperatures and salt conditions of the immobilization and preliminary incubation procedures of initial rounds: RNA and an excess of biotinylated oligonucleotide were denatured in water (3 minutes, 80°C) and allowed to cool for a brief period at room temperature before the addition of the non-magnesium components of the ligation buffer. After 10 minutes, MgCl₂ was added and the reaction was incubated another 10 minutes. The reaction was started by addition of substrate oligonucleotide and stopped with EDTA (100 mM). Prior to selection on the oligonucleotide affinity column, the stopped ligation mixture was passed through streptavidin-agarose beads to retain the pool RNA and wash off unreacted substrate. The pool RNA was then eluted from the column and selected as in Fig. 3. When the ligation reaction contained RNA from later rounds and was analyzed directly without enrichment for ligated molecules (for example, in the time courses of Figs. 4B, 5B, 6, and 7), the pool RNA was not typically annealed to the biotinylated oligonucleotide but instead was annealed to a non-biotinylated oligonucleotide of the same sequence.
 34. Phosphate compounds were detected with ammonium molybdate and reduced vanadyl chloride [R. M. C. Dawson, D. C. Elliott, W. H. Elliott, K. M. Jones, *Data for Biochemical Research* (Clarendon Press, Oxford, ed. 3, 1986), p. 486].
 35. G. Volckaert and W. Fiers, *Anal. Biochem.* **83**, 228 (1977).
 36. Pool DNA was amplified by PCR with the use of the biotinylated primer (30) that hybridizes to the 3' constant region of the pool DNA. After purification on an agarose gel, the PCR product was end-labeled. The biotin moiety at the 3' constant region of the pool RNA blocked labeling so that the DNA was labeled only on the end of the 5' constant region. Restriction digestions were performed in the presence of plasmid carrier DNA; monitoring the extent of the carrier DNA digestion confirmed that the digestions were complete.
 37. We thank R. Green for helpful discussions and J. R. Lorsch, K. B. Chapman, R. W. Roberts, and other members of the laboratory for careful reading of this manuscript. Supported by grants from Hoechst AG and NASA.

5 May 1993; accepted 25 June 1993

Physical Chemistry of the H₂SO₄/HNO₃/H₂O System: Implications for Polar Stratospheric Clouds

M. J. Molina, R. Zhang, P. J. Wooldridge, J. R. McMahan, J. E. Kim, H. Y. Chang, K. D. Beyer

Polar stratospheric clouds (PSCs) play a key role in stratospheric ozone depletion. Surface-catalyzed reactions on PSC particles generate chlorine compounds that photolyze readily to yield chlorine radicals, which in turn destroy ozone very efficiently. The most prevalent PSCs form at temperatures several degrees above the ice frost point and are believed to consist of HNO₃ hydrates; however, their formation mechanism is unclear. Results of laboratory experiments are presented which indicate that the background stratospheric H₂SO₄/H₂O aerosols provide an essential link in this mechanism: These liquid aerosols absorb significant amounts of HNO₃ vapor, leading most likely to the crystallization of nitric acid trihydrate (NAT). The frozen particles then grow to form PSCs by condensation of additional amounts of HNO₃ and H₂O vapor. Furthermore, reaction probability measurements reveal that the chlorine radical precursors are formed readily at polar stratospheric temperatures not just on NAT and ice crystals, but also on liquid H₂SO₄ solutions and on solid H₂SO₄ hydrates. These results imply that the chlorine activation efficiency of the aerosol particles increases rapidly as the temperature approaches the ice frost point regardless of the phase or composition of the particles.

Polar stratospheric clouds (PSCs) play a crucial role in the depletion of ozone (O₃) in the polar stratosphere in the winter and spring months: They promote the conversion of stable inorganic chlorine compounds

(ClONO₂ and HCl) into a photolytically active form (Cl₂), enabling the formation of the chlorine radicals Cl and ClO that participate in catalytic O₃ destruction processes (1, 2). Furthermore, the PSC particles facil-

Table 1. Spectral characteristics of the crystallized $\text{H}_2\text{SO}_4/\text{HNO}_3/\text{H}_2\text{O}$ solutions along with the amounts that could separate into SAT, NAT, and

ice by weight percent and information about spontaneous sample crystallization upon cooling to 190 K.

Sample number	Fraction in solution (%)		Partitioning (%)			Crystallized upon cooling	Dominant spectral signature	Other spectral features
	H_2SO_4	HNO_3	SAT	NAT	Ice			
1	47.5	9.5	82.4	17.6	0	No	$\text{H}_2\text{SO}_4 \cdot 4\text{H}_2\text{O}$	
2	44.1	12.6	76.5	23.4	0	No	$\text{H}_2\text{SO}_4 \cdot 4\text{H}_2\text{O}$	NAT
3	30	25.8	52	47.9	0	No	$\text{H}_2\text{SO}_4 \cdot 4\text{H}_2\text{O}$	NAT
4	45	6.8	78.1	12.6	9.3	No	None dominant	
5	39	10	67.7	18.6	13.8	No	None dominant	NAT
6	30	12.5	52	23.2	24.7	*	*	
7	23.8	19	41.3†	35.3†	23.4†	Yes	$\text{H}_2\text{SO}_4 \cdot 6.5\text{H}_2\text{O}$	NAT
8	40	6.6	69.4‡	12.3‡	18.4‡	Yes	$\text{H}_2\text{SO}_4 \cdot 6.5\text{H}_2\text{O}$	
9	22.3	24	38.7§	44.6§	16.7§	Yes	$\text{H}_2\text{SO}_4 \cdot 6.5\text{H}_2\text{O}$	NAT

*Never crystallized. †Or 52.1 percent $\text{H}_2\text{SO}_4 \cdot 6.5\text{H}_2\text{O}$; 35.3 percent NAT, and 12.6 percent ice. ‡Or 87.8 percent $\text{H}_2\text{SO}_4 \cdot 6.5\text{H}_2\text{O}$, 12.3 percent NAT, and 0 percent ice. §Or 55.1 percent $\text{H}_2\text{SO}_4 \cdot 8\text{H}_2\text{O}$, 44.6 percent NAT, and 0 percent ice.

itate the conversion of NO_2 to the stable species HNO_3 , which remains mostly in the condensed phase: Reduced NO_2 concentrations greatly increase the efficiency of O_3 destruction by Cl radicals because NO_2 reacts with ClO in the gas phase to form the stable species ClONO_2 .

Type I PSCs are generally believed to consist of nitric acid trihydrate (NAT), and to condense at temperatures 2 to 4 K above the frost point of water ice, whereas type II PSCs consist of ice particles and condense at temperatures just below the ice frost point (3). A common view is that the formation of PSCs involves the freezing of background sulfate aerosols, with solid sulfuric acid hydrates providing condensation nuclei for the NAT or ice particles (4). Other theories suggest that PSCs might consist of liquid or amorphous solid HNO_3 solutions (5, 6), or nitric acid dihydrate (NAD) (7), although all of these phases are thermodynamically less stable than NAT under polar stratospheric conditions.

In this article we present results of laboratory observations on liquid-solid transformations of the $\text{H}_2\text{SO}_4/\text{HNO}_3/\text{H}_2\text{O}$ system and on its chlorine activation properties. Previously, we investigated the gas-liquid equilibria for this ternary system (8) and concluded that the HNO_3 concentration in liquid stratospheric sulfate aerosols increases rapidly with decreasing temperature; the expected compositions are shown in Fig. 1 for three sets of stratospheric conditions, in which constant H_2O and HNO_3 mixing ratios are assumed for each line. In this study we used a variety of techniques to establish the identity of the solids that form when such ternary liquids freeze. Infrared (IR) spectroscopic, differential scanning calorimetric (DSC), and vapor pressure measurements yielded consistent results, namely that the solids formed

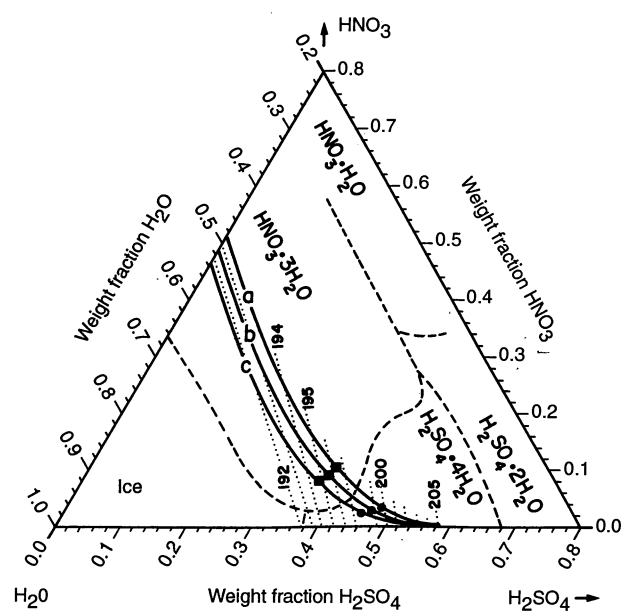
by freezing liquids with compositions corresponding to polar stratospheric conditions are NAT and H_2SO_4 hydrates. For compositions corresponding to temperatures below the ice frost point, ice also crystallizes from these solutions.

We also investigate the likelihood that solutions with various compositions and temperatures would freeze. Binary $\text{H}_2\text{SO}_4/\text{H}_2\text{O}$ solutions are prone to supercool: Our results indicate that $\text{H}_2\text{SO}_4/\text{H}_2\text{O}$ aerosols in the stratosphere would remain in liquid form unless they encounter temperatures a few degrees below the ice frost point. On the other hand, NAT forms readily from solutions containing sufficient HNO_3 , leading to the formation of PSCs at temperatures several degrees above the ice frost point.

Infrared spectra. Spectra of frozen ter-

nary samples were recorded with the same experimental technique that we used recently to study supercooled H_2SO_4 solutions and the crystalline hydrates (9). Briefly, solution films were held between 2.5-cm diameter AgCl windows separated by a 15- μm -thick Teflon spacer ring within a thermostated copper block. The spectra were measured with a Nicolet 800 Fourier transform spectrometer with a resolution of 2 cm^{-1} . The samples were chosen to be within the range of compositions expected for the winter polar stratosphere (similar to the solid lines of Fig. 1). The spectral characteristics of the crystallized samples are summarized in Table 1, along with the amounts that by mass conservation could separate into sulfuric acid tetrahydrate (SAT), NAT, and ice by weight percent

Fig. 1. Ternary diagram for the $\text{H}_2\text{SO}_4/\text{HNO}_3/\text{H}_2\text{O}$ system. Superimposed upon this figure are the dilution curves (solid lines) for liquid stratospheric aerosols at 100 mbar ($\sim 16\text{ km}$) and at ambient mixing ratios of 5 ppmv (parts per million by volume) H_2O and of (a) 10 ppbv HNO_3 , (b) 5 ppbv HNO_3 , and (c) 2.5 ppbv HNO_3 . Also shown along the dilution lines are the equilibrium temperatures (dotted lines), the frost points of crystalline $\text{HNO}_3 \cdot 3\text{H}_2\text{O}$ (that is, $S_{\text{NAT}} = 1$) (●), and the points at which the HNO_3 vapor pressure reaches supersaturations of 10 with respect to NAT ($S_{\text{NAT}} = 10$) (■). The temperatures and compositions of the dilution curves are calculated from our $\text{H}_2\text{SO}_4/\text{HNO}_3/\text{H}_2\text{O}$ vapor pressure data (8) and extrapolated below $\sim 195\text{ K}$ to the



intercepts on the $\text{HNO}_3/\text{H}_2\text{O}$ line as estimated from the vapor pressure data of Hanson (5). For (a), the $\text{HNO}_3/\text{H}_2\text{O}$ line is reached at 193.5 K; the ice frost point is 192.6 K for 5 ppmv H_2O at 100 mbar. The dashed curves are the eutectic lines reported by Carpenter and Lehrman (15); also indicated is the identity of the various solids that at equilibrium crystallize first upon cooling liquids with compositions bounded by the eutectic lines.

The authors are in the Department of Earth, Atmospheric, and Planetary Sciences and the Department of Chemistry, Massachusetts Institute of Technology, Cambridge, MA 02139.

(in this article, percentages refer to weight percent). Table 1 also provides information on whether the sample crystallized spontaneously upon cooling to 190 K (if not, then the sample had to be cooled to ≤ 150 K and warmed to ~ 190 K, sometimes repeatedly, to induce crystallization).

The IR spectra of various HNO_3 hydrates, especially NAT, have been investigated by several groups (10, 11). The initial disagreement between recent measurements of NAT spectra and earlier studies was probably largely due to different polymorphs forming under the different conditions, as nitrate crystals have a tendency to form numerous structures of similar stability (12). Our spectra of NAT films condensed from the vapor onto a single window at temperatures below 200 K does agree with the previously reported metastable form (10, 11); the stable form was generated upon warming to ≥ 210 K in a closed cell and did not change further with cooling and warming except to melt at ~ 254 K, as expected for NAT (13). The spectra obtained by freezing liquid samples were essentially the same as those obtained by condensing solids from the vapor, except that the stable form usually crystallized directly from the liquid without passing through a metastable phase.

Examples of the spectra acquired from the frozen solutions are depicted in Fig. 2, along with those of pure NAT, SAT, and SAH (sulfuric acid hemihydrate, $\text{H}_2\text{SO}_4 \cdot 6.5\text{H}_2\text{O}$). Generally, the first noticeable changes upon crystallization were the appearance of NAT bands at 820, 730, and 700 cm^{-1} (the stronger NAT band at 1378 cm^{-1} being initially obscured by sulfate absorptions). In no case were features observed that could not be accounted for in terms of ice, NAT, sulfuric acid hydrates (either SAT or SAH, depending on the liquid composition), or unfrozen ternary solutions.

Vapor pressures. We measured vapor pressures P_{HNO_3} and $P_{\text{H}_2\text{O}}$ for frozen $\text{H}_2\text{SO}_4/\text{HNO}_3/\text{H}_2\text{O}$ solutions in order to establish the identity of the solids formed. The apparatus has been described earlier (8, 9); briefly, it consists of a flow tube, whose walls are coated with the condensed phase of interest, attached to a mass spectrometer.

The results for a frozen solution containing 10 percent HNO_3 and 50 percent H_2SO_4 superimposed on a $\text{HNO}_3/\text{H}_2\text{O}$ phase diagram are shown in Fig. 3. The slope in the plot of $\log P_{\text{HNO}_3}$ versus $\log P_{\text{H}_2\text{O}}$ at a given temperature is -3 , demonstrating the presence of NAT, as inferred from the Gibbs-Duhem equation. Furthermore, the vapor pressure values agree well with those reported originally by Hanson and Mauersberger for NAT (14). The experimental data presented in Fig. 3 are also shown in Fig. 4,

superimposed on a $\text{H}_2\text{SO}_4/\text{H}_2\text{O}$ phase diagram. Vapor pressure measurements carried out with ternary solutions of various other initial compositions yielded similar results: The solids formed are some combination of ice, H_2SO_4 hydrates, and HNO_3 mono- and trihydrate with vapor pressures equal to those of the hydrates formed separately in each of the two binary systems.

Calorimetry. We used differential scanning calorimetry (DSC) to measure phase transition temperatures, including melting points, for frozen ternary solutions with compositions similar to those used in the Fourier transform IR spectroscopy and mass spectrometry investigations. The experimental technique has been described earlier (9).

The DSC warming curves for four frozen

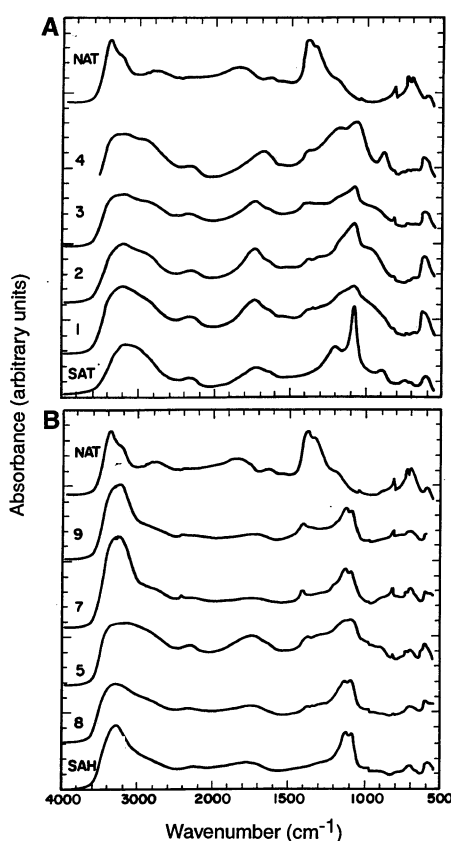


Fig. 2. Infrared spectra of various crystallized $\text{H}_2\text{SO}_4/\text{HNO}_3/\text{H}_2\text{O}$ solutions. The spectra of pure NAT, SAT, and SAH also frozen from solution are shown for comparison. The numbers correspond to those given in Table 1. The spectra of samples 1 to 4 resemble SAT with minor amounts of NAT, and possibly with some liquid, particularly in sample 4. Sample 5 has prominent NAT bands; the principal sulfate stretching region, 1000 to 1300 cm^{-1} , does not show unambiguously whether SAT, SAH, or liquid H_2SO_4 is present, but the overall spectrum most nearly resembles SAT. Samples 7 and 9 clearly have characteristics of both NAT and SAH. The NAT bands are very slightly present, if at all, in samples 1, 4, and 8, but these samples are the most dilute in nitric acid.

samples are shown in Fig. 5. The results indicate the presence of NAT and H_2SO_4 hydrates in the ternary samples. We found no evidence for the formation of mixed $\text{H}_2\text{SO}_4\text{-HNO}_3$ hydrates from these and other solutions with concentrations varying from 0 to 40 percent HNO_3 and from 30 to 50 percent H_2SO_4 . If the samples are rapidly frozen (for example, with liquid nitrogen), glasses with arbitrary compositions can form, but these crystallize upon warming to 180 to 190 K, yielding the binary hydrates. Our results are in good agreement with the melting point determinations of Carpenter and Lehman (15), who concluded that there are no mixed hydrates for the entire range of possible compositions in the $\text{H}_2\text{SO}_4/\text{HNO}_3/\text{H}_2\text{O}$ ternary system. Their eutectic lines bounding the stability regimes of different hydrates are shown as dashed lines in Fig. 1, which shows the $\text{H}_2\text{SO}_4/\text{HNO}_3/\text{H}_2\text{O}$ ternary diagram.

Supercooling experiments. We investigated the supercooling behavior of various acid solutions with sizes ranging from 5 μl to 3 ml. Two types of experiments were carried out: point of freezing determinations of samples cooled at a constant rate (typically 2 degrees per minute), and the length of time required for freezing of samples held at a constant temperature. For smaller samples the phase change was detected by monitoring the transmission of light from a helium-neon laser; for larger samples it was detected by monitoring the rapid temperature increase accompanied with crystallization.

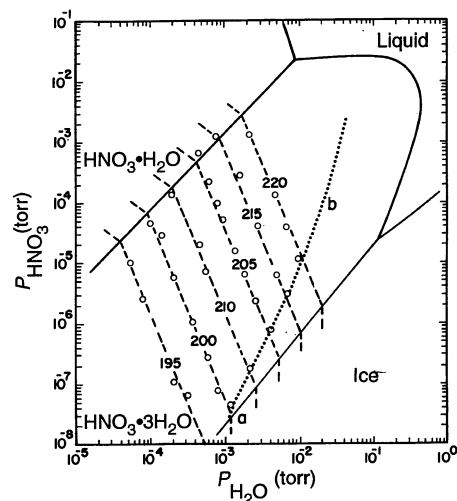


Fig. 3. Vapor pressures over crystallized ternary solutions superimposed on a phase diagram of the $\text{HNO}_3/\text{H}_2\text{O}$ system. The solid lines represent equilibrium conditions for the coexistence of two condensed phases, and the dashed lines are isotherms. The open circles represent the experimental points for a sample obtained by freezing a 50 percent H_2SO_4 and 10 percent HNO_3 solution. The dotted line corresponds to temperatures and H_2O vapor pressures for the freezing envelope of $\text{H}_2\text{SO}_4 \cdot 4\text{H}_2\text{O}$ (9).

Solutions of H_2SO_4 supercool readily (16). Our results show that 3-ml samples of $\text{H}_2\text{SO}_4/\text{H}_2\text{O}$ solutions with acid concentrations from 50 to 70 percent do not freeze, even after being held for more than 24 hours at temperatures between 203 and 230 K. Classical nucleation theory indicates that smaller samples require longer times to freeze; these times are inversely proportional to the volume. Calculations by Luo *et al.* (17) yielded homogeneous freezing times from 1 to 10 hours for 0.1- μm droplets under similar temperature and concentration conditions. However, as pointed out by these authors, the calculations are highly

sensitive to the assumed values of the diffusion activation energy, which characterizes the homogeneous nucleation process; our results suggest that this energy is most likely larger than their estimate. Also, atmospheric observations indicate that H_2SO_4 aerosols remain liquid down to temperatures as low as 192 K (18, 19).

Ternary $\text{H}_2\text{SO}_4/\text{HNO}_3/\text{H}_2\text{O}$ solutions are observed to freeze readily if their concentrations correspond to those predicted for supercooled sulfate aerosols at temperatures approaching the ice frost point (8). Table 2 summarizes the results of our observations for the 3-ml samples whose compo-

sitions fall on line a in Fig. 1, which corresponds to ambient mixing ratios of 5 parts per million by volume (ppmv) H_2O and 10 ppbv HNO_3 at 100 mbar (~ 16 -km altitude). The data show that a 1-degree change in temperature has a large effect on the freezing probability as a consequence of the effect on the equilibrium composition, particularly at lower temperatures. In contrast, for samples of a given composition the freezing probability is hardly affected by a 1-degree change in the temperature at which the observations are carried out.

It is difficult to tell which particular hydrate forms first when the ternary solutions listed in Table 2 freeze; in most cases, the entire sample crystallizes rapidly. The reason is that in the ternary system the formation of one of the hydrates causes a shift in the composition of the remaining liquid toward more extensive supercooling with respect to the other hydrate. An alternative explanation is that the first hydrate formed provides nucleation centers for the other one; however, we find from seeding experiments in supercooled binary solutions that H_2SO_4 hydrates are not good nuclei for NAT, and vice versa. On the other hand, the IR data discussed above suggest that NAT nucleates first for some of the samples investigated.

In order to elucidate the effect of HNO_3 on the supercooling behavior of stratospheric sulfate aerosols, we also investigated the freezing characteristics for samples without HNO_3 , that is, for $\text{H}_2\text{SO}_4/\text{H}_2\text{O}$ solutions with compositions corresponding to the same water partial pressure and the same equilibrium temperatures T_{eq} as those ternary solutions listed in Table 2 (the compositions fall on the $\text{H}_2\text{SO}_4/\text{H}_2\text{O}$ axis in Fig. 1). These results show that, for $T_{\text{eq}} > 196$ K, the effect of HNO_3 on supercooling is not statistically significant. In contrast, for $T_{\text{eq}} < 196$ K, none of the $\text{H}_2\text{SO}_4/\text{H}_2\text{O}$ samples froze, whereas most of the ternary samples did freeze. Hence, the presence of HNO_3 in the liquid aerosols at concentrations corresponding to those in the polar stratosphere promotes freezing very efficiently, particularly at temperatures approaching the ice frost point.

Experiments carried out with 5- μl and 3-ml samples show that $\text{H}_2\text{SO}_4/\text{H}_2\text{O}$ solutions with concentrations close to the ice/SAT eutectic (~ 40 percent H_2SO_4) rarely freeze, and normally form a glass upon cooling down to 150 K. Samples with H_2SO_4 concentration below 35 percent begin to freeze readily; such concentrations correspond to equilibrium temperatures several degrees below the ice frost point.

Although our supercooling experiments suggest the probable freezing behavior of stratospheric aerosols, they do not provide definitive quantitative information. This is

Fig. 4. Water vapor pressures over crystallized ternary solutions superimposed on a phase diagram for the $\text{H}_2\text{SO}_4/\text{H}_2\text{O}$ system. The solid lines represent equilibrium conditions for the coexistence of two condensed phases, and the dashed lines are isotherms. The open circles are the same as in Fig. 3. The dotted line represents conditions corresponding to the equilibrium coexistence of $\text{HNO}_3 \cdot 3\text{H}_2\text{O}$ and $\text{HNO}_3 \cdot \text{H}_2\text{O}$ (14). The H_2O vapor pressures and temperatures defining the line a-b are the same as in Fig. 3; it corresponds to the freezing envelope of SAT (9). In these isothermal experiments, a readjustment of the H_2O partial pressure in the flow tube is followed by a corresponding change in the HNO_3 vapor pressure on a time scale of less than 1 min; the conversion of "H₂O-rich" to "HNO₃-rich" NAT requires only a minor change in the composition of the hydrate (26). In contrast, a phase transition—such as melting, or conversion to a different hydrate—usually requires a significant amount of one of the components to be condensed or evaporated, and hence, a larger response time, easily observable in our experiments. Such a situation arises when the H_2O partial pressure reaches the values represented by the line a-b: melting of SAT at constant temperature and $P_{\text{H}_2\text{O}}$ is accompanied by the condensation of H_2O vapor, because under those conditions the mole fraction of H_2O in the liquid in equilibrium with SAT is significantly greater than 4:1.

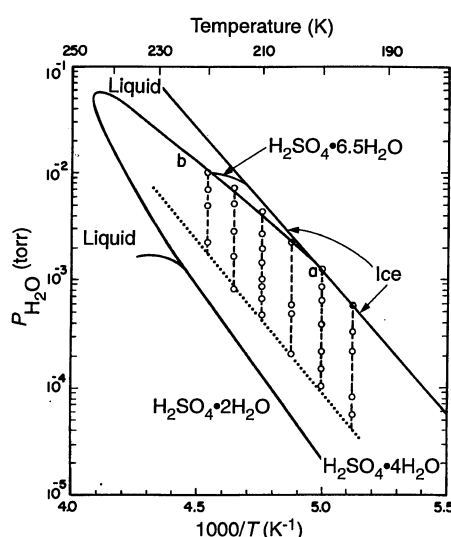
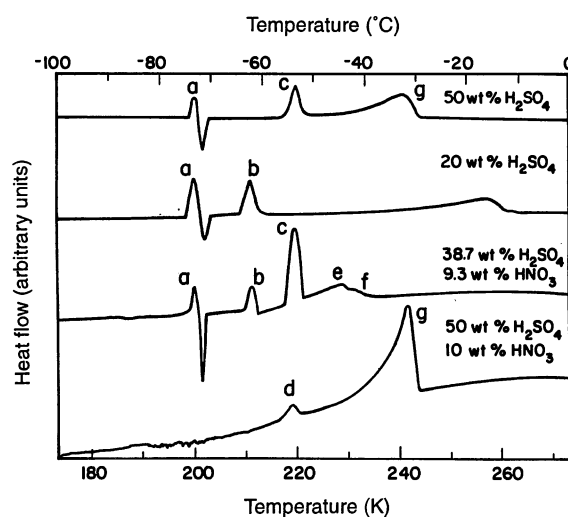


Fig. 5. A series of DSC warming curves showing melting of crystallized $\text{H}_2\text{SO}_4/\text{HNO}_3/\text{H}_2\text{O}$ samples. Also shown for comparison are the two upper traces are the warming curves of 20 and 50 percent H_2SO_4 solutions (9). For the sample with 38.7 percent H_2SO_4 and 9.3 percent HNO_3 the solid-solid phase transition temperatures match closely those of the $\text{H}_2\text{SO}_4/\text{H}_2\text{O}$ binary system (32): the peaks marked a near 200 K represent either the eutectic melting of ice/ H_2SO_4 tetrahydrate (SAT) followed by crystallization into H_2SO_4 hemihexahydrate (SAH), or the solid-solid conversion of octahydrate into SAH; the coexistence mixture of ice/SAH has an eutectic near 211 K (peak b), which is little changed in the ternary eutectic; and the peritectic transformation of SAH to SAT occurs at 219 K (peak c), which is again essentially the same in the binary and ternary systems. The two small peaks (e and f) correspond to the melting of SAT at 230 K and NAT at 233 K, respectively. For the sample with 50 percent H_2SO_4 and 10 percent HNO_3 , the peak d at 220 K most likely represents the eutectic melting of NAT and SAT, which is followed by the melting of SAT near 240 K (peak g).



a consequence of the stochastic nature of the nucleation process, the different time scales and larger sample sizes in our laboratory work, and the identity of the crystallization nuclei, if any. However, our results do provide upper limits to probable freezing temperatures because the effects of glass surfaces, impurities, and large sample sizes can only increase the nucleation rate. Our data indicate that a large fraction of the H_2SO_4 aerosols remains in liquid form until they reach the polar stratosphere, and that the aerosols are likely to freeze at temperatures a few degrees above the ice frost point, forming NAT and H_2SO_4 hydrates.

PSC formation mechanism. If an air parcel in the stratosphere cools and becomes supersaturated with respect to the formation of NAT for H_2O and HNO_3 vapors, the liquid $\text{H}_2\text{SO}_4/\text{HNO}_3/\text{H}_2\text{O}$ aerosol droplets in the parcel become supersaturated with respect to crystallization of NAT out of this solution. This follows from the experimental observations that essentially pure NAT crystallizes from the ternary solutions, and from the fact that in a multicomponent-multiphase system at equilibrium the chemical potential of each component is the same in all phases. Furthermore, the nucleation barrier for the formation of a NAT embryo in the liquid phase should be smaller than in the gas phase. Hence, the most likely first step in the formation of type I PSCs consists of crystallization of NAT out of liquid aerosol droplets.

Atmospheric observations (18, 20) indicate that the formation of PSCs requires supersaturation ratios S_{NAT} as large as 10 with respect to NAT in terms of the HNO_3 partial pressure in the Arctic stratosphere.

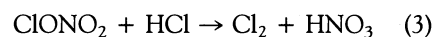
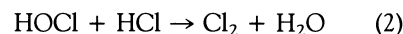
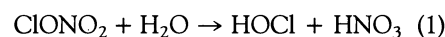
These observations do not discriminate between a liquid-solid and a gas-solid nucleation mechanism. They are, however, compatible with our proposed mechanism, in light of the observed supercooling behavior for the ternary $\text{H}_2\text{SO}_4/\text{HNO}_3/\text{H}_2\text{O}$ solutions: NAT crystallization occurs readily for compositions and temperatures corresponding to $S_{\text{NAT}} \geq 10$. As is shown in Fig. 1, cooling from 196.5 to 193.5 K along line a changes the equilibrium HNO_3 concentrations from 10.4 percent to ~49 percent (S_{NAT} increases from 10 to ~90); that is, the equilibrium composition of the liquid droplets changes very rapidly as the ice frost point is approached. Hence, temperature fluctuations in the stratosphere are likely to induce crystallization, not because of the increase in the degree of supercooling for droplets of a given composition, but because of the change in the equilibrium composition: As the H_2SO_4 concentration decreases and the HNO_3 concentration increases the solutions crystallize more readily.

The most commonly suggested PSC formation mechanism (4) assumes that frozen sulfate aerosols—consisting presumably of crystalline H_2SO_4 hydrates—provide the nuclei for the condensation of NAT. Our seeding experiments have shown that SAT crystals are not efficient nuclei for NAT crystallization in supercooled 3:1 $\text{H}_2\text{O}/\text{HNO}_3$ solutions. Hence, it appears unlikely for NAT crystals to condense on SAT crystals directly from the vapor phase. Similarly, other PSC formation mechanisms suggesting the condensation of liquid or amorphous solid $\text{H}_2\text{O}/\text{HNO}_3$ solutions as a first step (5, 6) appear implausible: HNO_3 is much more likely to condense on preexist-

ing liquid particles, a process that does not require nucleation. Furthermore, amorphous solid solutions are unstable at stratospheric temperatures: they can only be generated in the laboratory at much lower temperatures, and they crystallize spontaneously upon warming. In addition, these phases are metastable with respect to NAT: In the stratosphere they would evaporate at temperatures several degrees below the NAT saturation point.

Worsnop *et al.* (7) recently proposed that type I PSCs may consist of NAD in addition to the more stable NAT. Their conclusions are based on laboratory studies of deposition of HNO_3 and H_2O vapors on ice and HNO_3 monohydrate solids deposited on a coated glass surface: NAD nucleates readily in its stability regime and persists even under conditions where it is metastable with respect to NAT. We did not observe NAD formation in our experiments involving nucleation from the liquid phase; furthermore, IR spectroscopic data show that NAD surfaces convert to NAT surfaces upon exposure to stratospheric water partial pressures (11).

Chlorine activation on sulfuric acid aerosols. The most important heterogeneous reactions responsible for transforming stable chlorine reservoir compounds into the photolytically active forms are the following:



The reaction probability (γ) for these processes has been measured in the laboratory on ice and on NAT surfaces under temperature and reactant partial pressure conditions approaching those found in the polar stratosphere (21, 22): the γ values have been found to be greater than 0.1 for reactions 1 to 3. Reaction 1 has also been investigated on liquid H_2SO_4 solutions (23); the rate depends strongly on the acid concentration ($\gamma \approx 0.1$ and 10^{-4} for 40 and 60 percent H_2SO_4 , respectively). Above 200 K, reactions 2 and 3 occur at negligible rates on stratospheric sulfate aerosols (23), because the H_2SO_4 concentration in the liquid aerosols is relatively large and the HCl solubility relatively small (8). On the other hand, the equilibrium HCl concentration in the liquid aerosols increases rapidly at lower temperatures (8), and hence these reactions are expected to proceed at significantly higher rates (24).

We have measured γ on SAT for reactions 2 and 3 under conditions characteristic of the polar stratosphere: that is, at temperatures between 190 and 200 K and at partial pressures of $\sim 10^{-7}$ torr for ClONO_2 and HCl, and of $\sim 10^{-4}$ torr for H_2O . The

Table 2. Freezing behavior of supercooled $\text{H}_2\text{SO}_4/\text{HNO}_3/\text{H}_2\text{O}$ solutions.

H_2SO_4 (%)	HNO_3 (%)	T_{eq}^* (K)	T_{exp}^\dagger (K)	Number of samples		Time to freeze (hour)	Observation time (hour)
				Frozen	Total		
39.4	8.9	197.0	188	5	5	0.6–1.6	—
39.4	8.9	197.0	195	0	8		27
36.9	10.9	196.3	189	9	14	0.5–19	24
36.9	10.9	196.3	195	2	10	10–40	40
35.5	12.1	196.0	196	8	14	5–31	48
35.5	12.1	196.0	188	4	5	<24	27
33.2	13.9	195.5	195	2	3	18–19	43
33.2	13.9	195.5	188	4	4	1–16	—
30.7	16.0	195.0	195	16	17	0.4–41	43
27.9	18.4	194.5	195	8	11	1–30	35
24.8	21.1	194.0	195	9	11	0.2–15	35
21.2	24.2	193.5	194	7	7	0.1–3.6	—
0.0	48.8	193.2	195	7	7	<0.2	—
47.4	0.0	197.0	196	2	4	2–4.6	24
46.3	0.0	196.4	195	3	4	1.7–5.4	24
45.7	0.0	196.0	197	1	4	6.5	24
40.8–	0.0	193.5–	195–	0	20		24
44.8		195.5	198				

*Equilibrium temperature corresponding to trace a in Fig. 1, except for the last four entries, which correspond to the $\text{H}_2\text{SO}_4/\text{H}_2\text{O}$ axis. †Temperature at which the sample was held (fluctuated by ± 1 K).

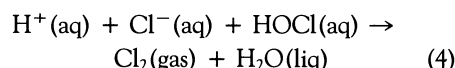
experimental technique is similar to the one described previously (22). Briefly, a jacketed flow tube with moveable injectors is coated with a liquid film of the solution of interest and is subsequently frozen; the flow tube is attached to a mass spectrometer that monitors the concentrations of reactants and products as a function of the injector position. Our earlier investigations of these reactions on NAT surfaces showed a strong dependency of γ on $P_{\text{H}_2\text{O}}$ (22); as expected, a similar situation applies for SAT, the water-rich crystals showing γ values comparable to those of ice ($\gamma > 0.1$) for reactions 2 and 3, whereas the values for the H_2SO_4 -rich crystals are two orders of magnitude smaller.

We have also carried out preliminary measurements of γ on liquid $\text{H}_2\text{SO}_4/\text{HCl}/\text{H}_2\text{O}$ films (25). For solutions containing between 38 and 60 percent H_2SO_4 and 0.01 percent HCl, the γ values were observed to be >0.1 at 220 K. In the stratosphere, we predict that the HCl concentration on liquid droplets should be >0.01 percent at temperatures below 198 K, assuming an ambient HCl partial pressure of 1.5×10^{-7} torr at 100 mbar (8). Thus chlorine activation by liquid aerosols should proceed readily in the polar stratosphere, even in the absence of PSCs.

Our results indicate that chlorine activation in the stratosphere can occur efficiently on a variety of surfaces, including ice, NAT, SAT, and liquid H_2SO_4 solutions. The requirement is a sufficiently low temperature for significant HCl uptake to take place, that is, roughly $T < 200$ K; this temperature is determined by the H_2O and HCl partial pressures prevailing in the stratosphere. Hence, PSCs are not essential for chlorine activation, although they facilitate this process by providing surface areas larger than those available from stratospheric background aerosols alone and by removing HNO_3 from the gas phase.

We believe that the mechanism for these reactions is essentially the same on the various surfaces that we investigated: It involves as a necessary step incorporation of HCl vapor into the surface layers of the aerosol particle and solvation to form aqueous ions. We have suggested that in the presence of HCl a liquid-like layer forms at the surface of the solid particles in which HCl solvation occurs (26, 27). Such a liquid-like layer is thought to exist on pure ice at temperatures down to ~ 240 K (28); it is thermodynamically stable because the sum of the surface free energies of the solid-liquid and liquid-gas interfaces is smaller than the surface free energy of the solid-gas interface. The freezing point of a 25 percent aqueous HCl solution is 187 K, so that a liquidlike HCl solution layer may indeed form on the surfaces of PSC particles

under stratospheric conditions. Our proposed mechanism for reactions 2 and 3 includes the following step, which occurs after HCl uptake and solvation in the liquid-like layer:



An alternative mechanism that has been suggested involves molecular adsorption of the reactants at the surface of the solid particles, with Langmuir adsorption isotherms, competition for active sites, and so forth (29). However, from a chemical bonding point of view, the energy involved in such adsorption should be at most 30 kJ/mol, corresponding to the formation of a strong hydrogen bond between HCl and the ice surface; the consequence of such a small interaction energy would be the incorporation of negligible amounts of HCl at the surface of the cloud particles under stratospheric conditions (26, 30). In contrast, if the HCl molecules are completely surrounded by water molecules with appropriate orientations they dissociate, releasing ~ 75 kJ/mol. This HCl solvation energy is large enough to rationalize the laboratory measurements, namely, that the amount of HCl taken up by ice surfaces under similar conditions corresponds to a coverage of the order of one-tenth of a monolayer (21, 22, 27, 31). Solvation of significant amounts of HCl is only possible in the presence of a quasi-liquid layer because the orientational freedom of water molecules in ice crystals is rather limited. If a liquid-like film consisting of several molecular layers is formed, the HCl concentration in that film would be 10 to 40 percent, and the HCl would be fully ionized (31). Furthermore, laboratory investigations of reaction 3 on the surfaces of true liquid HCl solutions in that concentration range yield essentially the same γ values as those measured on ice or NAT surfaces in the presence of HCl vapor at partial pressures of the order of 10^{-7} to 10^{-8} torr (26, 27). Thus the availability of water at the particle surfaces, which increases rapidly as the ice frost point is approached, may facilitate these heterogeneous reactions through solvation of the acid species.

REFERENCES AND NOTES

- S. Solomon, R. R. Garcia, F. S. Rowland, D. J. Wuebbles, *Nature* **321**, 755 (1986); S. Solomon, *Rev. Geophys.* **26**, 131 (1988); J. G. Anderson, D. W. Toohey, W. H. Brune, *Science* **251**, 39 (1991); W. H. Brune *et al.*, *ibid.* **252**, 1260 (1991); M. J. Molina, *Atmos. Environ.* **25A**, 2535 (1991).
- M. J. Molina, T.-L. Tso, L. T. Molina, F. C.-Y. Wang, *Science* **238**, 1253 (1987).
- M. P. McCormick, H. M. Steele, P. Hamill, W. P. Chu, T. J. Swisler, *J. Atmos. Sci.* **39**, 1397 (1982); O. B. Toon, P. Hamill, R. P. Turco, J. Pinto, *Geophys. Res. Lett.* **13**, 1283 (1986); P. J. Crutzen and F. Arnold, *Nature* **324**, 651 (1986).
- L. R. Poole and M. P. McCormick, *J. Geophys. Res.* **93**, 8423 (1987); P. Hamill, R. P. Turco, O. B. Toon, *J. Atmos. Chem.* **7**, 287 (1988); S. C. Wosfy, R. J. Salawitch, M. B. McElroy, *J. Atmos. Sci.* **47**, 2004 (1990).
- D. R. Hanson, *Geophys. Res. Lett.* **17**, 421 (1990).
- F. Arnold, *Ber. Bunsenges. Phys. Chem.* **96**, 334 (1992).
- D. R. Worsnop, L. E. Fox, M. S. Zahniser, S. C. Wosfy, *Science* **259**, 71 (1993).
- R. Zhang, P. J. Wooldridge, M. J. Molina, *J. Phys. Chem.* **97**, 8541 (1993).
- R. Zhang, P. J. Wooldridge, J. P. D. Abbatt, M. J. Molina, *ibid.*, p. 7351.
- G. Ritzhaupt and J. P. Devlin, *ibid.* **95**, 90 (1991); M. A. Tolbert and A. M. Middlebrook, *J. Geophys. Res.* **95**, 22423 (1991); R. H. Smith, M. T. Leu, L. F. Keyser, *J. Phys. Chem.* **95**, 5924 (1991); B. G. Koehler, A. M. Middlebrook, M. A. Tolbert, *J. Geophys. Res.* **97**, 8065 (1992).
- A. M. Middlebrook, B. G. Koehler, L. S. McNeill, M. A. Tolbert, *Geophys. Res. Lett.* **19**, 2417 (1992).
- See, for example, Z. X. Shen, M. Huok, S. H. Tang, *Spectrochim. Acta* **48A**, 1317 (1992), and references therein.
- W. R. Forsythe and W. F. Giauque, *J. Am. Chem. Soc.* **64**, 48 (1942).
- D. R. Hanson and K. Mauersberger, *Geophys. Res. Lett.* **15**, 855 (1988).
- C. D. Carpenter and A. Lehman, *Trans. Am. Inst. Chem. Eng.* **17**, 35 (1925).
- C. M. Gable, H. F. Betz, S. H. Maron, *J. Am. Chem. Soc.* **72**, 1445 (1950); G. C. Vuillard, *Ann. Chim.* **13**, 233 (1957); T. Ohtake, *Tellus* **45B**, 138 (1993).
- B. P. Luo, Th. Peter, P. J. Crutzen, *Ber. Bunsenges. Phys. Chem.* **96**, 334 (1992).
- J. E. Dye *et al.*, *J. Geophys. Res.* **97**, 8015 (1992).
- R. F. Pueschel *et al.*, *ibid.* **97**, 8105 (1992); O. Toon *et al.*, *Science* **261**, 1136 (1993).
- S. R. Kawa *et al.*, *J. Geophys. Res.* **97**, 7925 (1992).
- D. R. Hanson and A. R. Ravishankara, *ibid.* **96**, 5081 (1991); M. T. Leu, S. B. Moore, L. F. Keyser, *J. Phys. Chem.* **95**, 7763 (1991).
- J. P. D. Abbatt and M. J. Molina, *J. Phys. Chem.* **96**, 7674 (1992).
- D. R. Hanson and A. R. Ravishankara, *J. Geophys. Res.* **96**, 17307 (1991); D. M. Golden, J. A. Manion, C. M. Reihns, M. A. Tolbert, in *CHEMRAWN VII: Chemistry of the Atmosphere: The Impact of Global Change*, J. G. Calvert, Ed. (Blackwell, Oxford, in press).
- M. J. Molina, in *Proceedings of the Joint Symposium on Ozone Depletion, Greenhouse Gases, and Climate Change* (National Academy Press, Washington, DC, 1989), pp. 48–55; E. W. Wolff, R. Mulvaney, K. Oates, *Geophys. Res. Lett.* **16**, 487 (1989); R. Turco and P. Hamill, *Ber. Bunsenges. Phys. Chem.* **96**, 323 (1992).
- J. Abbatt, J. McMahon, M. J. Molina, *Eos* **73**, 634 (1992).
- M. J. Molina, in *CHEMRAWN VII: Chemistry of the Atmosphere: The Impact of Global Change*, J. G. Calvert, Ed. (Blackwell, Oxford, in press).
- J. Abbatt *et al.*, *J. Geophys. Res.* **97**, 15,819 (1992).
- H. H. G. Jellinek, *J. Colloid Sci.* **25**, 192 (1967); P. V. Hobbs, *Ice Physics* (Clarendon, Oxford, 1974).
- S. Elliott, R. P. Turco, O. B. Toon, P. Hamill, *J. Atmos. Chem.* **13**, 211 (1991); M. Mozurkewich, *Geophys. Res. Lett.* **20**, 355 (1993).
- G. J. Kroes and D. C. Clary, *Geophys. Res. Lett.* **19**, 1355 (1992).
- A. Tabazadeh and R. P. Turco, *J. Geophys. Res.* **98**, 12,727 (1993).
- W. F. Giauque, E. W. Hornung, J. E. Kunzler, T. R. Ruben, *J. Am. Chem. Soc.* **82**, 62 (1960).
- Supported by an NSF grant (ATM-9017150) and a NASA grant (NAG2-632) to the Massachusetts Institute of Technology. R.Z. is supported by a NASA graduate fellowship.

18 May 1993; accepted 9 August 1993